Charge-exchange EUV spectroscopy in collisions of Xe^{q+} (q = 7–9) with rare gases

H. Tanuma* and H. Ohashi†
Department of Physics, Tokyo Metropolitan University, 1-1 Minami-Ohsawa, Hachioji, Tokyo 192-0397, Japan

N. Yamamoto,‡ D. Kato, and I. Murakami
National Institute for Fusion Science, 322-6 Oroshi-cho, Toki 509-5292, Japan

S. Fujioka, H. Nishimura, and K. Nishihara
Institute of Laser Engineering, Osaka University, 2-6 Yamada-oka, Suita, Osaka 565-0871, Japan
(Received 20 September 2011; published 28 October 2011; publisher error corrected 2 November 2011)

Extreme ultraviolet (EUV) emission spectra have been measured in charge exchange collisions between Xe^{q+} (q = 7–9) and rare gases at an energy of 20 q keV. We have observed 4, 22, and 39 lines in collisions of Xe^{7+}, Xe^{8+}, and Xe^{9+}. Of these emission lines, four lines of Xe VII, eight lines of Xe VIII, and nine lines of Xe IX correspond to newly observed transitions. The identification procedure is described in detail. The aim of this work is to obtain spectroscopic data for multiply charged Xe ions. In addition, the electron capture mechanism is also discussed using the crude classical over-the-barrier model to understand the target dependence of the emission spectra.

DOI: 10.1103/PhysRevA.84.042713 PACS number(s): 34.70.+e, 32.30.−r

I. INTRODUCTION

Charge exchange processes in collisions of multiply charged ions with neutral atoms are extensively investigated both theoretically and experimentally as one of the most active research subjects in atomic physics. Photon-emission spectroscopy (PES), in other words, charge exchange spectroscopy (CXS), in which the line intensities of radiation are measured following the charge transfer reaction in collisions of multiply charged ions with neutral target gases, is mainly used for cross-section measurements of these processes [1–3]. It is, however, also a very powerful experimental tool to investigate the transition energies and energy levels of multiply charged ions [4–6].

Much effort has recently been focused on the development of an EUV light source for next-generation photolithography, which is one of the key technologies in the manufacturing of semiconductor devices [7]. One of the candidates for use in high power EUV light sources is xenon plasma produced by a laser or gas discharge. Detailed spectroscopic data on multiply charged xenon ions are necessary to understand the physics of the xenon plasma. The available spectroscopic information on xenon ions, however, is fairly limited at this moment. Published work on xenon ions through December 2002 was compiled by Saloman [8]. Even in this most detailed article about the energy levels and spectral lines of xenon ions, the number of levels and lines are relatively few and not nearly as complete for the multiply charged states. After the publishing of this article, some works have also been performed on xenon ions using electron beam ion traps (EBIT) [9–12]. The EBIT is a powerful device which is suitable for the production of highly charged ions, but it is difficult to measure the emission lines from individual charge states of less than 10+ for xenon using an EBIT.

In this study, we have measured the EUV emission spectra from excited multiply charged xenon ions produced in charge exchange collisions of Xe^{q+} (q = 7–9) with rare gases to provide fundamental spectroscopic data for xenon ions. We have already reported preliminary results on collisions of Xe ions with He, in which both the spectral resolution and the S/N in the spectra were not sufficient to enable a detailed analysis [13]. Since then we have improved the quality of the measurements as reported in this work.

Total cross sections for electron capture in slow collisions of multiply charged xenon ions with rare gases have been reported in several articles [14–19]. Most of those studies, however, have been performed for highly charged ions $q \geqslant 10$ or $q \geqslant 15$. For q = 7–9, single and double electron capture have been measured in collisions with He at 0.5 and 1.0 keV/q [14]. At these energies, single-electron capture (SEC) is the most dominant, and cross sections for true double-electron capture (TDC) are much smaller than those for SEC and also smaller than those for transfer ionization (TI). After charge exchange collisions with He, most projectile charge is reduced by 1, resulting from both SEC and TI. In the collisions with other rare gas atoms, however, TDC should be taken into consideration. Furthermore, charge exchange spectroscopy has been performed in collisions of Xe^{q+} (q = 6–8) with He at an energy of 10–15q keV [4,5]. The photon emission in this work, however, has been observed in a wavelength region longer than 35 nm, and the observation regions have no overlap with that in this study. Generally, the features from the charge transfer process in keV collisions do not depend sensitively on the collision energy. Therefore we can assume the same characteristics will be obtained here as the collision processes reported at different energies.

The features of the capture levels and the capture cross sections in low-energy collisions of multiply charged ions with neutral atoms and molecules can be explained qualitatively by the classical over-the-barrier (COB) model [20–22]. This

*tanuma-hajime@tmu.ac.jp
†Present address: Institute for Laser Science, University of Electro-Communications, Chofu, Tokyo 182-8585, Japan.
‡Present address: Chubu University, Kasugai, Aichi 487-0027, Japan.

model gives the principal quantum number of the dominant capture orbital as

$$n_{\mathrm{cap}} \approx \left[\frac{1+2\sqrt{q}}{2I_t\,(q+2\sqrt{q})}\right]^{\frac{1}{2}} q, \qquad (1)$$

where q is the charge state of the incident ion, and I_t is the ionization energy of the target in atomic units. This model assumes hydrogenic energy levels and the existence of pure Coulomb potentials between the ionic core and the outer active electrons. However, even the most highly charged ion in this work, namely Xe^{9+}, has 45 electrons, and its energy levels are very far from hydrogenic. For such lowly charged ions, the COB model is not appropriate to describe the electron transfer reactions quantitatively. Even though the COB model is not sufficiently accurate to explain the detailed mechanism of the collision processes, the qualitative understanding provided by this model is quite useful for the consideration of the experimental results, such as the charge-state dependence and the target dependence. In this study, we have used five kinds of rare gases as targets, which have quite different ionization energies, namely 24.5874 eV for He, 21.5646 eV for Ne, 15.7596 eV for Ar, 13.9996 eV for Kr, and 12.1298 eV for Xe, with the expectation of strong target dependence in the emission spectra.

II. EXPERIMENT

The multiply charged xenon ions were produced in an electron cyclotron resonance (ECR) ion source [23] with an injection of xenon gas and heating by microwaves of 14.25 GHz. To increase the ion intensity, oxygen gas was also injected into the plasma chamber of the ion source. The xenon ions were extracted with an electric potential of 20 kV and selected by a 110° double-focusing dipole magnet according to their charge-to-mass ratios m/q. The beam of ions with a diameter of about 6 mm was directed into a collision chamber, where it interacted with an effusive gas beam from a multicapillary plate at 90°. Ion beam currents were measured by a Faraday cup located behind the collision region. Typical mean ion currents during the experiment were 0.1–1 μA, and the target gas pressure in the collision chamber was held below 1×10^{-4} Pa to maintain the single-collision conditions. In this experiment, however, it was difficult to measure the absolute value of the target gas pressure in the collision region. Therefore we do not derive absolute cross sections for the charge exchange reaction and the radiation emission in this paper.

Optical radiation in the EUV region from the collision center was observed at 90° to both the ion beam and the gas jet with a compact flat-field grazing-incident spectrometer (SSK-260, Shin Seiki Co.) equipped with a toroidal-type converging mirror and a variable line space (ca. 1200 lines/mm) grating blazed at 100 nm. A liquid nitrogen cooled CCD camera (C4880, Hamamatsu) was installed in the spectrometer as a photon detector to observe and accumulate emission lines in the wavelength range of 6–24 nm simultaneously. The typical exposure time was 12 hours for each spectrum, and the spectra were corrected for many cosmic ray events. Also the intensity of the observed emission was corrected with the consideration of the quantum yield of the CCD which depends on the wavelength.

In the spectrometer, an adjustable slit was positioned between the converging mirror and the grating. Slit widths of 200 and 500 μm gave us the mean resolutions of 0.03 and 0.10 nm, respectively. The calibration of wavelengths was performed with the observation of more than 20 emission lines of O VI and O VII in collisions of O^{6+} and O^{7+} with Xe gas. The uncertainty of the observed wavelength measurements was estimated at 0.02 nm.

III. RESULTS AND DISCUSSION

A. Emission spectra in collisions of Xe^{7+}

Figure 1 shows the observed emission spectra in collisions of Xe^{7+} with Ar, Kr, and Xe target gases. In the cases of He and Ne targets, no emission lines have been observed in the

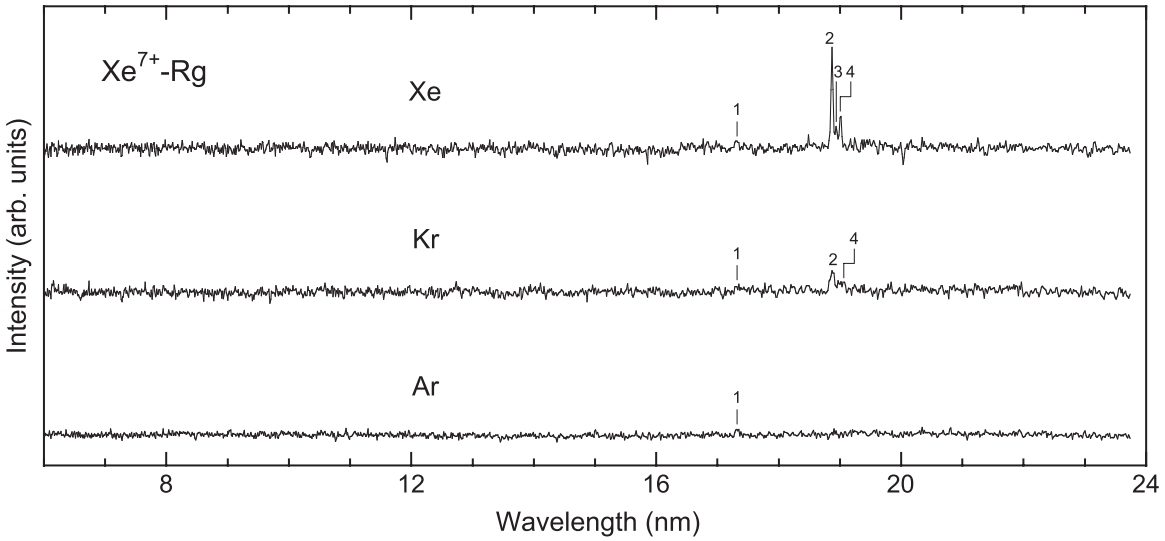

FIG. 1. EUV emission spectra of radiation resulting from the collisions of Xe^{7+} with Ar, Kr, and Xe at an energy of 140 keV. The mean resolution is 0.1 nm for Ar and Kr targets and 0.03 nm for the Xe target.

TABLE I. Observed emission lines in collisions of Xe^{7+} with Ar, Kr, and Xe at energies of 140 keV. λ_{obs}: the averaged wavelength of the observed emission line. λ_{level}: the wavelength of the emission line derived from the difference between energy levels of Xe VII compiled in Ref. [8]. $\Delta\lambda$: the wavelength difference between the λ_{obs} and λ_{level}.

	Target								
No.	Ar	Kr	Xe	λ_{obs} (nm)	Charge state	λ_{level} (nm)	Lower state	Upper state	$\Delta\lambda$ (nm)
1	17.30	17.31	17.32	17.31	VII	17.339	$5p^2\ ^3P_1$	$4d^9 5s^2 4f\ ^1P_1^\circ$	0.04
2		18.84	18.84	18.84	VII		$5s^2\ ^1S_0$	$5s7p\ ^1P_1^\circ$	
3			18.91	18.91	VII	18.891	$5s^2\ ^1S_0$	$5s7p\ ^3P_2^\circ$	0.02
4		18.99	18.98	18.98	VII	18.957	$5s^2\ ^1S_0$	$5s7p\ ^3P_1^\circ$	0.02
						18.973	$5s^2\ ^1S_0$	$5s7p\ ^3P_0^\circ$	0.01
						18.979	$5s6s\ ^3S_1$	$4d^9 5s^2 5f\ ^3P_1^\circ$	0.00

wavelength region from 6–24 nm. A very weak emission line has been observed at 17.30 nm in the collisions of Xe^{7+} with Ar, Kr, and Xe, and three lines around 18.9 nm have also been observed in spectra with heavier atom targets. The emission lines at 18.84 and 18.98 nm could be observed with two targets, but the line at 18.91 nm could not be distinguished in the case of the Kr target because of insufficient spectral resolution.

In charge exchange collisions of Xe^{7+} with a neutral gas target, Xe VII and Xe VI are the product ions from single and double electron capture, respectively. In the wavelength region between 6.0 and 23.7 nm, nine lines of Xe VII and no line of Xe VI have been compiled in Ref. [8]. We, however, could not find any transitions corresponding to the four emission lines observed here in these data. Using the tables of energy levels of Xe VII and Xe VI in Ref. [8], however, we have tried to seek out transition wavelengths which are coincident with those of the observed lines. The results are summarized and shown in Table I. The wavelength $\lambda = 18.98$ nm agrees with the transitions of $5s^2\ ^1S_0$–$5s7p\ ^3P_1$ and $5s^2\ ^1S_0$–$5s7p\ ^3P_0$ within the uncertainty of the measurement. This line also coincides with the position of the $5s6s\ ^3S_1$–$4d^9 5s^2 5f\ ^3P_1$ transition. The line at $\lambda = 18.91$ nm is considered as the transition of $5s^2\ ^1S_0$–$5s7p\ ^3P_2$ after comparison with the wavelengths derived from the known energy levels.

On the other hand, we could not find the transitions corresponding to both the dominant peak at $\lambda = 18.84$ nm and the small peak at $\lambda = 17.30$ nm from the difference of the energy levels. We suggest that the $\lambda = 18.84$ nm line is identified as the $5s^2\ ^1S_0$–$5s7p\ ^1P_1$ transition. This identification gives the energy level of $5s7p\ ^1P_1$ as $53\,080 \pm 30$ cm^{-1}.

Generally speaking, the LS coupling scheme is not appropriate for the heavy atoms, and it might be better to use j-j coupling to describe the electronic states. We know that the intermediate coupling scheme is the most appropriate one for xenon ions. However, the LS terms are very useful to explain the relative transition probabilities with consideration according to the selection rules for the electronic dipole transitions, namely $\Delta S = 0$, $\Delta L = 0, \pm 1$ (except between

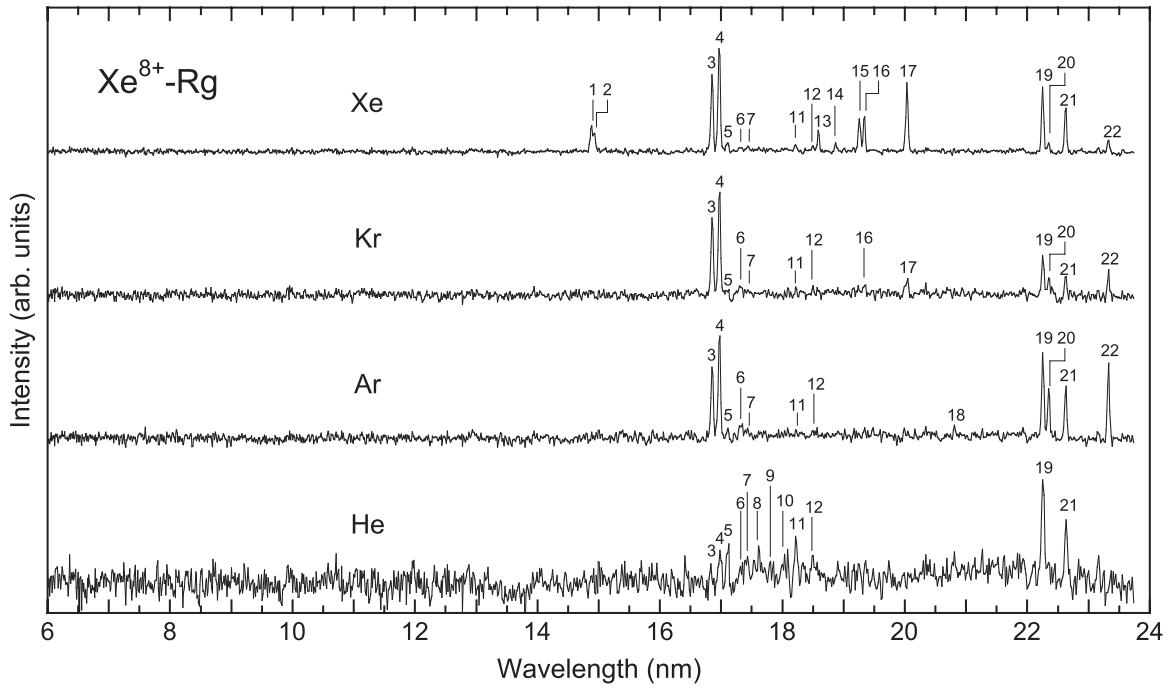

FIG. 2. EUV emission spectra of radiation resulting from the collisions of Xe^{8+} with He, Ar, Kr, and Xe at the energy of 160 keV. The mean resolution is 0.03 nm for all target gases.

S states), and $\Delta J = 0, \pm 1$ (except between $J = 0$ states). Actually, the relative intensities of three $5s$-$7p$ lines observed in collisions of Xe^{7+} with Xe have shown a tendency to obey the electronic dipole transition selection rules; only the prominent line of $^1S_0$–$^1P_1$ is optically allowed, and the other two weak lines corresponding to the singlet–triplet transitions are not only spin-forbidden but also forbidden with respect to the total angular momentum J.

The $\lambda = 17.30$ nm line is close to the value of 17.339 nm reported for the $5p^2\ ^3P_1$–$4d^9 5s^2 4f$ transition, but this upper state is difficult to populate from the $Xe^{7+}(4d^{10}5s\ ^2S_{1/2})$ by the charge transfer reaction. Therefore, we regard this line as a resonance line from a $5snl$ ($nl > 7p$) state which has not yet been observed elsewhere. In summary, all four lines of Xe VII in this work are newly observed.

B. Emission spectra in collisions of Xe^{8+}

EUV emission spectra resulting from collisions of Xe^{8+} with He, Ar, Kr, and Xe are shown in Fig. 2. Twenty-two emission lines have been observed in these spectra. In Ref. [8], 16 lines have been compiled as the transitions of Xe VII between 6.0 and 23.7 nm. A comparison of the observed emission lines in Fig. 2 with the established transition lines of Xe VIII and Xe VII is shown in Table II. In this table, we have also shown the wavelengths derived from the energy differences between known levels of Xe VIII and VII.

Nine of the 22 observed lines are identified as known transitions of Xe VIII, even though other assignments are possible for five lines. The weak $\lambda = 17.30$ and 18.84 nm lines are the same as those observed in collisions of Xe^{7+}, and these are regarded as the emission from Xe VII which is produced in the double-electron capture of Xe^{8+}. The 17.79 nm line has two candidates for corresponding transitions. On the other hand, the lines at 18.19 and 20.77 nm have no convincing identification. As the final result, we have concluded that at least nine lines are observed as new transitions of Xe VIII in this work.

The 22.20 and 22.58 nm lines are observed in all four spectra of Fig. 2, and the intensity ratio of these two lines is almost the same and close to 2:1. This finding indicates that both lines correspond to the $5s - 6p$ transitions from the different fine-structure levels of $J = 3/2$ and $1/2$. The same trend is found in the 14.87 and 14.91 nm lines which correspond to the $5s$–$8p$ transitions. On the other hand, the $5s$–$7p$ transitions, at 16.82 and 16.95 nm, have anomalous intensity ratios in all four spectra (i.e., the emission from $J = 1/2$ is stronger than that from $J = 3/2$). This finding will be discussed later.

According to the above considerations, we conclude that the dominant emission lines in the EUV region correspond to

TABLE II. Observed emission lines in collisions of Xe^{8+} with He, Ar, Kr, and Xe at energies of 160 keV. λ_{obs}: the averaged wavelength of the observed emission line. λ_{line}: the wavelength of the known transition line. λ_{level}: the wavelength of the emission line derived from the difference between energy levels of Xe VIII and Xe VII compiled in Ref. [8]. $\Delta\lambda$: the wavelength differences between λ_{obs} and λ_{line} or between the λ_{obs} and λ_{level}.

	Target										
No.	He	Ar	Kr	Xe	λ_{obs} (nm)	Charge state	λ_{line} (nm)	λ_{level} (nm)	Lower state	Upper state	$\Delta\lambda$ (nm)
1				14.87	14.87	VIII		14.877	$5s\ ^2S_{1/2}$	$8p\ ^2P_{3/2}$	0.01
2				14.91	14.91	VIII		14.927	$5s\ ^2S_{1/2}$	$8p\ ^2P_{1/2}$	0.02
3	16.80	16.83	16.83	16.83	16.82	VIII		16.841	$5s\ ^2S_{1/2}$	$7p\ ^2P_{3/2}$	0.02
4	16.96	16.95	16.95	16.95	16.95	VIII		16.954	$5s\ ^2S_{1/2}$	$7p\ ^2P_{1/2}$	0.00
5	17.09	17.08	17.08	17.08	17.08	VIII	17.086		$5s\ ^2S_{1/2}$	$4d^9(^2D_{5/2})5s5p(^1P_1^\circ)\ (5/2,^1P_1^\circ)_{3/2}$	0.01
6	17.30	17.30	17.30	17.30	17.30[a]	VII					
7	17.39				17.39	VII		17.382	$5p^2\ ^1D_2$	$4d^9 5s^2 4f\ ^1P_1$	0.01
8	17.59				17.59	VIII	17.587		$5s\ ^2S_{1/2}$	$4d^9(^2D_{3/2})5s5p(^3P_2^\circ)\ (3/2,^3P_2^\circ)_{1/2}$	0.00
9	17.79				17.79	VIII	17.771		$5s\ ^2S_{1/2}$	$4d^9(^2D_{3/2})5s5p(^3P_1^\circ)\ (3/2,^3P_1^\circ)_{3/2}$	0.02
						VIII		17.805	$5p\ ^2P_{3/2}$	$8d\ ^2D_{5/2}$	0.02
10	18.01				18.01	VIII	18.014		$5s\ ^2S_{1/2}$	$4d^9(^2D_{5/2})5s5p(^3P_2^\circ)\ (5/2,^3P_2^\circ)_{1/2}$	0.00
11	18.19				18.19[b]						
12	18.45	18.47	18.47	18.48	18.47	VIII	18.466		$5s\ ^2S_{1/2}$	$4d^9(^2D_{5/2})5s5p(^3P_1^\circ)\ (5/2,^3P_1^\circ)_{3/2}$	0.00
13				18.56	18.56	VIII		18.569	$5p\ ^2P_{1/2}$	$8s\ ^2S_{1/2}$	0.01
14				18.84	18.84[a]	VII					
15				19.22	19.22	VIII		19.232	$5p\ ^2P_{3/2}$	$8s\ ^2S_{1/2}$	0.01
16			19.30	19.30	19.30	VIII		19.300	$5p\ ^2P_{1/2}$	$7d\ ^2D_{3/2}$	0.00
17			19.98	19.99	19.99	VIII		19.988	$5p\ ^2P_{3/2}$	$7d\ ^2D_{5/2}$	0.00
18		20.77			20.77[b]						
19	22.20	22.21	22.21	22.21	22.20	VIII	22.218		$5s\ ^2S_{1/2}$	$6p\ ^2P_{3/2}$	0.00
20		22.30	22.30	22.30	22.30	VIII	22.279		$5p\ ^2P_{1/2}$	$7s\ ^2S_{1/2}$	0.02
21	22.58	22.58	22.57	22.57	22.58	VIII	22.554		$5s\ ^2S_{1/2}$	$6p\ ^2P_{1/2}$	0.02
22		23.27	23.27	23.27	23.27	VIII	23.243		$5p\ ^2P_{3/2}$	$7s\ ^2S_{1/2}$	0.03

[a]These emission lines are also observed in collisions of Xe^{7+}.

[b]The convincing identification has not been found yet.

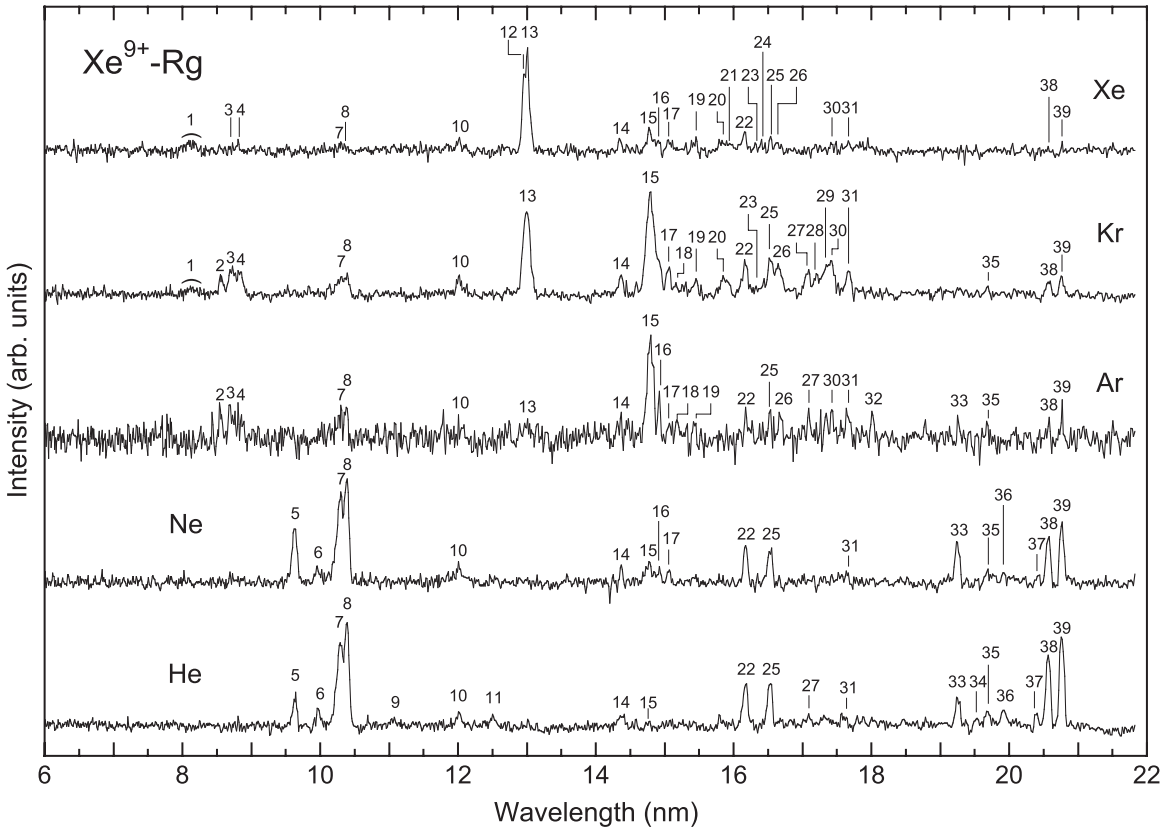

FIG. 3. EUV emission spectra of radiation resulting from the collisions of Xe^{9+} with He, Ne, Ar, Kr, and Xe at an energy of 180 keV. The mean resolution is 0.1 nm for He, Ne, and Kr targets, and 0.03 nm for Ar and Xe targets.

optical transitions of Xe VIII from collisions of Xe^{8+} with rare gases, even though the emission from Xe VII is observed with very small intensity.

As can be seen in Fig. 2, the emission spectra in collisions of Xe^{8+} depend significantly on the target. In the spectrum obtained with an He target, the $5s$–$6p$ transitions are prominent. The emissions from the 7ℓ states, however, are dominant in the spectrum with an Ar target. Furthermore, in the case of the Xe target, the emissions of the $5s$–$8p$ and $5p$–$8s$ transitions have significant intensities in the observed spectrum. Such a tendency can be understood with the classical over-the-barrier model because these targets have different ionization energies and the dominant capture levels should be different.

C. Emission spectra in collisions of Xe^{9+}

Figure 3 shows the emission spectra recorded in the wavelength region between 6.0 and 21.8 nm observed in collisions of Xe^{9+} with He, Ne, Ar, Kr, and Xe. In the spectrum measured with the spectrometer used in this study, lines from second-order diffraction are also observed with strong intensity. Hence, we must account for emission at 2λ in the longer wavelength region for lines emitted at the wavelength of λ. In Fig. 3, nine lines could be identified as second-order lines.

Only 12 lines have been compiled as transitions of Xe IX in the wavelength region below 21.8 nm in Ref. [8]. On the other hand, 30 emission lines have been observed in collisions of Xe^{9+}, except the nine lines due to second-order diffraction. In Fig. 3, it is difficult to distinguish the emission lines at 15.95 nm in the Xe target spectrum and 17.35 nm in the Ar target one. We have, however, noted that these two lines were observed at the corresponding positions on the CCD images. The wavelengths of the observed lines and their identifications are shown in Table III. To draw up the table, we have considered not only the emission wavelengths of the known transitions of Xe IX and Xe VIII, but also the wavelengths derived from the energy differences between two levels of Xe IX and Xe VIII.

As shown in this table, we have observed all of the 12 known transitions of Xe IX and five new lines of Xe IX. Also one new line of Xe VIII is observed and identified. For ten observed lines, namely 8.18, 11.04, 15.45, 15.84, 15.95, 17.20, 17.35, 18.01, 19.52, and 19.68 nm, we could not find the appropriate transitions corresponding to them. The ionization energies of Xe VIII and Xe IX are known to be 105.976 ± 0.04 and 179.85 ± 0.10 eV, respectively [8]. These energies correspond to 11.70 and 6.89 nm, respectively. Therefore, since they are shorter than 11.70 nm and longer than 6.89 nm, the 8.18 and 11.04 nm lines are assigned as emission lines of Xe IX.

The emission line of 13.0 nm observed in collisions of Xe^{9+} with Kr and Xe targets has a much larger linewidth than the spectral resolution of the spectrometer used in this work. We confirm that this line consists of at least two individual lines, which are resolved in spectra from an Xe target recorded with a higher resolution of 0.03 nm. According to Hebrew University Lawrence Livermore Atomic Code (HULLAC) calculations, the 13.0 nm line corresponds to more than a dozen transitions between $4d^9 5s$ and $4d^9 8p$ states.

TABLE III. Observed emission lines in collisions of Xe^{9+} with He, Ne, Ar, Kr, and Xe at energies of 180 keV. λ_{obs}: the averaged wavelength of the observed emission line. λ_{line}: the wavelength of the known transition line. λ_{level}: the wavelength of the emission line derived from the difference between energy levels of Xe IX and Xe VIII compiled in Ref. [8]. $\Delta\lambda$: the wavelength differences between λ_{obs} and λ_{line} or between λ_{obs} and λ_{level}.

No.	Target					λ_{obs} (nm)	Charge state	λ_{line} (nm)	λ_{level} (nm)	Lower state	Upper state	$\Delta\lambda$ (nm)
	He	Ne	Ar	Kr	Xe							
1				8.18	8.18	8.18[a,b]	IX[c]					
2			8.56	8.56		8.56	IX	8.542		$4d^{10}\,{}^1S_0$	$4d^9 6f\,{}^1P_1$	0.02
3			8.72	8.73	8.73	8.73	IX	8.752		$4d^{10}\,{}^1S_0$	$4d^9 7p\,{}^1P_1$	0.02
4			8.87	8.84	8.81	8.84	IX	8.844		$4d^{10}\,{}^1S_0$	$4d^9 7p\,{}^3P_1$	0.00
5	9.64	9.63				9.63	IX	9.645		$4d^{10}\,{}^1S_0$	$4d^9 5f\,{}^1P_1$	0.02
6	9.97	9.96				9.97	IX	9.955		$4d^{10}\,{}^1S_0$	$4d^9 5f\,{}^3D_1$	0.01
7	10.30	10.30	10.27	10.29	10.29	10.29	IX	10.282		$4d^{10}\,{}^1S_0$	$4d^9 6p\,{}^1P_1$	0.01
8	10.39	10.39	10.38	10.39	10.40	10.39	IX	10.381		$4d^{10}\,{}^1S_0$	$4d^9 6p\,{}^3P_1$	0.01
9	11.04					11.04[a]	IX[c]					
10	12.02	12.01	12.01	12.02	12.01	12.01	IX	12.013		$4d^{10}\,{}^1S_0$	$4d^9 4f\,{}^1P_1$	0.00
11	12.51	12.51				12.51	IX		12.517	$4d^{10}\,{}^1S_0$	$4d^9 5d\,{}^3P_0$	0.01
12					12.96	12.96	IX			$(4d^9 5s$	$4d^9 8p)$[d]	
13			12.99	13.00	13.01	13.00	IX			$(4d^9 5s$	$4d^9 8p)$[d]	
14	14.37	14.37	14.37	14.37	14.35	14.37	IX	14.361		$4d^{10}\,{}^1S_0$	$4d^9 4f\,{}^3D_1$	0.01
15	14.78	14.78	14.80	14.80	14.78	14.79[e]	IX		14.767	$4d^9 5s\,{}^3D_3$	$4d^9 7p\,{}^3P_1$	0.02
							IX			$(4d^9 5s$	$4d^9 7p)$[d]	
16		14.93	14.92		14.92	14.92	IX		14.945	$4d^9 5s\,{}^3D_2$	$4d^9 7p\,{}^1P_1$	0.03
17		15.06	15.07	15.06	15.05	15.06	IX	15.028		$4d^{10}\,{}^1S_0$	$4d^9 4f\,{}^3P_1$	0.03
18			15.18	15.16		15.17	IX		15.137	$4d^9 5s\,{}^3D_1$	$4d^9 7p\,{}^3P_1$	0.03
19			15.44	15.45	15.46	15.45[a]						
20				15.85	15.84	15.84[a]						
21					15.95	15.95[a]						
22	16.18	16.18	16.18	16.18	16.16	16.17	IX	16.174		$4d^{10}\,{}^1S_0$	$4d^9 5p\,{}^3D_1$	0.00
23				16.33	16.32	16.32		8.16×2				
24					16.41	16.41		8.21×2				
25	16.53	16.53	16.53	16.54	16.54	16.54	IX	16.532		$4d^{10}\,{}^1S_0$	$4d^9 5p\,{}^1P_1$	0.01
26			16.68	16.65	16.63	16.65	VIII		16.654	$5p\,{}^2P_{3/2}$	$9d\,{}^2D_{5/2}$	0.00
							VIII		16.662	$5p\,{}^2P_{3/2}$	$9d\,{}^2D_{3/2}$	0.01
27			17.09	17.09		17.09		8.542×2				
28				17.20		17.20[a]						
29			17.35	17.35		17.35[a]						
30			17.43	17.39	17.42	17.41		8.752×2				
31	17.60	17.65	17.66	17.67	17.67	17.67		8.844×2				
32			18.01			18.01[a]						
33	19.25	19.25	19.25			19.25		9.645×2				
34	19.52					19.52[a]						
35	19.68	19.68	19.68	19.68		19.68[a]						
36	19.92	19.92				19.92		9.955×2				
37	20.39	20.42				20.41	IX		20.415	$4d^9 5s\,{}^1D_2$	$4d^9 6p\,{}^3P_1$	0.01
38	20.56	20.56	20.58	20.57	20.56	20.57		10.282×2				
39	20.76	20.76	20.77	20.76	20.76	20.76		10.381×2				

[a]The convincing identification has not been found yet.
[b]For this very weak and broad peak, the wavelength is determined as the average of two corresponding second-order lines.
[c]The charge state is determined from the ionization energies of Xe VIII and Xe IX.
[d]The identification is due to the HULLAC calculation.
[e]Accidental overlap with the other transitions is suggested because of the extremely large linewidth.

The 14.8 nm line can be also resolved into two lines with 0.03 nm resolution in spectra with an Ar target. However, one of the lines still has a large width of 0.10 nm. To explain this, we propose the overlap of some unresolved lines with an extremely short lifetime of the excited state. Assuming the convolution of two Gaussians, the FWHM of this line, 0.10 nm, and the resolution of 0.03 nm give a natural width of 0.095 nm, which corresponds to an energy width of 0.54 eV and a lifetime of about 1.2×10^{-15} s. As shown in Table III, we have identified this line as the $5s\,{}^3D_3$–$7p\,{}^3P_1$ transition. Even if this identification were correct, the lifetime of 1.2 fs is unrealistically short. Therefore, we propose that more than

ten unresolved lines of the $4d^9 5s$–$4d^9 7p$ transitions compose this broad peak on the basis of the HULLAC calculation.

As can be seen in Fig. 3, the emission spectra in collisions of Xe^{9+} show very strong target dependence. The emissions from the 5ℓ and 6ℓ states are dominant in the spectra recorded with He and Ne targets. On the other hand, emissions from the $7p$ state, instead of the $6p$ state, are prominent in the cases of Ar and Kr targets.

D. Charge exchange processes

According to Ref. [4], the single-electron capture to the $n = 5$ levels is the most dominant process in collisions of both Xe^{7+} and Xe^{8+} with He. However, the emissions from the 5ℓ states of Xe^{6+} and Xe^{7+} have longer wavelengths than the range observed in this work.

We have observed that the $7p$ states are populated sufficiently in the Xe^{7+}–Xe collisions. Although the most dominant n has not been measured, it is likely to be 7 or 6. Using Eq. (1), the COB model predicts that $n = 3.7$ and 5.3 are the dominant levels in collisions of Xe^{7+} with He and Xe, respectively. Therefore we can suggest that the COB model gives smaller values of n_{cap} than the experimental results. The COB model has been developed for bare or extremely highly charged ions. Therefore the discrepancy from the experiments can be understood as the screening effect of the electrons.

Emission spectra in collisions of Xe^{8+} have indicated that the dominant n is equal to, or smaller than, 6 for the He target, and it is probably 7 for other heavy targets. The COB values n_{cap} are given by Eq. (1) as 4.2, 5.2, 5.5, and 5.9 for He, Ar, Kr, and Xe targets. Here the differences of n between the observation and the calculation are also 1 or 2. Therefore we can expect that the target dependence is explained with the COB model after some modification.

The n_{cap} in the COB model are 4.6, 4.9, 5.7, 6.1, and 6.5 in collisions of Xe^{9+} with He, Ne, Ar, Kr, and Xe. For the lighter four targets, the relation between the COB model and the observation seems to be same as mentioned above. That is to say, the $4d$–$6p$ lines are strong in the case of He and Ne targets and weak with the heavier targets, and on the other hand, the $4d$–$7p$ and $5s$–$8p$ lines are observed with significant intensities with only heavier targets.

In the emission lines from $Xe^{7+}(np\ ^2P_J)$ in collisions of Xe^{8+}, the intensity ratios of the $5s\ ^2S_{1/2}$–$np\ ^2P_{3/2}$ to the $5s\ ^2S_{1/2}$–$np\ ^2P_{1/2}$ have been measured for $n = 6$–8. According to the statistical weights of the fine-structure levels, the ratios should be exactly 2 for all n. The experimental result for $n = 7$ was, however, about 0.7 and this is very far from the theoretical expectation. We have also measured the intensity ratio of the $7s\ ^2S_{1/2}$–$7p\ ^2P_{3/2}$ (351.16 nm) to the $7s\ ^2S_{1/2}$–$7p\ ^2P_{1/2}$ (407.90 nm) by using the UV-visible spectrometer [24]. The result for the $7s$–$7p$ transitions showed good agreement with that for the $5s$–$7p$ transitions in the EUV region. Therefore the initial populations of the $7p$ fine-structure levels produced by the charge transfer reaction are different from their statistical weights. The reason might lie in the mechanism of the charge exchange reaction including the strong spin-orbit interaction due to heavy xenon ions. However, the detailed mechanism of this phenomenon needs to be investigated by theoretical calculations.

ACKNOWLEDGMENTS

The authors would like to thank Dr. Akira Sasaki, Professor Fumihiro Koike, Professor Takeshi Kagawa, Professor Takako Kato, and other members of the EUV modeling group organized by one of the authors (KN) for fruitful discussions. Also the authors are deeply grateful to Professor Gerard O'Sullivan and Dr. Rebekah D'Arcy for the critical reading of the paper. This work was financially supported, in part, by MEXT (Ministry of Education, Culture, Sports, Science, and Technology, Japan) under contract subject "Leading Project for EUV lithography source development." And a part of this work was performed under the collaboration program of the Institute of Laser Engineering, Osaka University.

[1] Y. S. Gordeev, D. Dijkkamp, A. G. Drentje, and F. J. de Heer, Phys. Rev. Lett. **50**, 1842 (1983).
[2] D. Dijkkamp, D. Ciric, E. Vlieg, A. de Boer, and F. de Heer, J. Phys. B **18**, 4763 (1985).
[3] G. Lubinski, Z. Juhasz, R. Morgenstern, and R. Hoekstra, J. Phys. B **33**, 5275 (2000).
[4] M. Druetta and D. Hitz, Nucl. Instr. Meth. B **98**, 211 (1995).
[5] M. O. Larsson, A. M. Gonzalez, R. Hallin, F. Heijkenskjold, R. Hutton, A. Langereis, B. Nystrom, G. O'Sullivan, and A. Wannstrom, Phys. Scr. **51**, 69 (1995).
[6] M. O. Larsson, A. M. Gonzalez, R. Hallin, F. Heijkenskjold, B. Nystrom, G. O'Sullivan, C. Weber, and A. Wannstrom, Phys. Scr. **53**, 317 (1996).
[7] V. Bakshi, *EUV Sources for Lithography* (SPIE, Bellingham, WA, 2006).
[8] E. B. Saloman, J. Phys. Chem. Ref. Data **33**, 765 (2004).
[9] E. Träbert, P. Beiersdorfer, J. K. Lepson, and H. Chen, Phys. Rev. A **68**, 042501 (2003).
[10] K. Fahy *et al.*, J. Phys. D **37**, 3225 (2004).
[11] C. Biedermann, R. Radtke, G. Fussmann, J. L. Schwob, and P. Mandelbaum, Nucl. Instr. Meth. B **235**, 126 (2005).
[12] K. Fahy, E. Sokell, G. O'Sullivan, A. Aguilar, J. M. Pomeroy, J. N. Tan, and J. D. Gillaspy, Phys. Rev. A **75**, 032520 (2007).
[13] H. Tanuma, H. Ohashi, E. Shibuya, N. Kobayashi, T. Okuno, S. Fujioka, H. Nishimura, and K. Nishihara, Nucl. Instr. Meth. B **235**, 331 (2005).
[14] E. Justiniano, C. L. Cocke, T. J. Gray, R. Dubois, C. Can, W. Waggoner, R. Schuch, H. Schmidt-Böcking, and H. Ingwersen, Phys. Rev. A **29**, 1088 (1984).
[15] H. Andersson, G. Astner, and H. Cederquist, J. Phys. B **21**, L187 (1988).
[16] H. Cederquist, Phys. Rev. A **43**, 2306 (1991).

[17] H. Cederquist *et al*., Phys. Rev. A **46**, 2592 (1992).
[18] N. Selberg, C. Biedermann, and H. Cederquist, Phys. Rev. A **54**, 4127 (1996).
[19] N. Selberg, C. Biedermann, and H. Cederquist, Phys. Rev. A **56**, 4623 (1997).
[20] H. Ryufuku, K. Sasaki, and T. Watanabe, Phys. Rev. A **21**, 745 (1980).
[21] A. Barany, G. Astner, H. Cederquist, H. Danared, S. Huldt, P. Hvelplund, A. Johnson, H. Knudsen, L. Liljeby, and K.-G. Rensfelt, Nucl. Instr. Meth. B **9**, 397 (1985).
[22] A. Niehaus, J. Phys. B **19**, 2925 (1986).
[23] H. Tanuma, J. Matsumoto, T. Nishide, H. Shiromaru, and N. Kobayashi, J. Chin. Chem. Soc. **48**, 389 (2001).
[24] H. Ohashi, Ph.D. Thesis, Tokyo Metropolitan University, 2010.